iScience

CellPress
OPEN ACCESS

Article

Thermodynamic modeling of *in-situ* rocket propellant fabrication on Mars

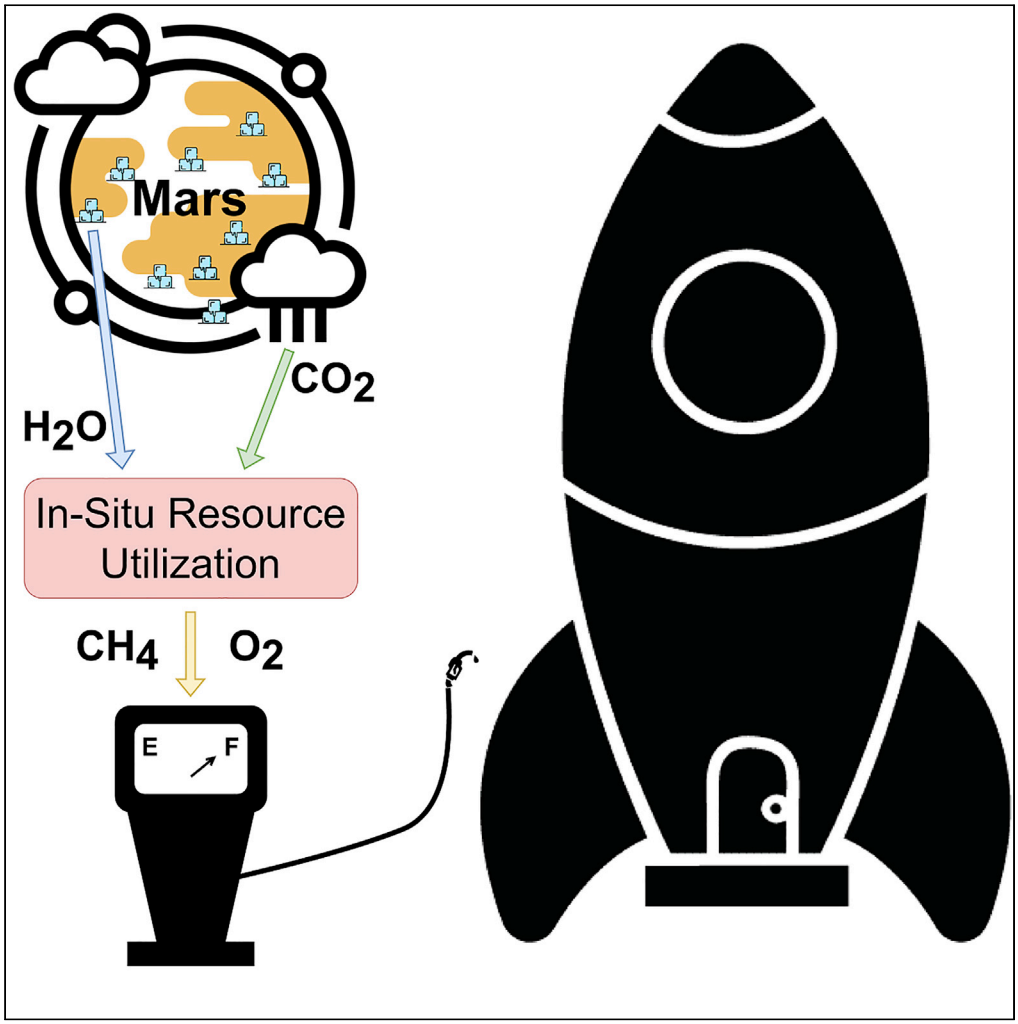

Shah Saud Alam, Christopher Depcik, Sindhu Preetham Burugupally, Jared Hobeck, Ethan McDaniel

depcik@ku.edu

Highlights

In-situ production of rocket propellants on Mars is possible

The second law of thermodynamics validates ISRU proof of concept

The proposed system can refuel rockets in 16 months (NASA goal)

The system is scalable and upgradable to a higher TRL

Alam et al., iScience *25*, 104323
May 20, 2022
https://doi.org/10.1016/j.isci.2022.104323

iScience

CellPress
OPEN ACCESS

Article

Thermodynamic modeling of *in-situ* rocket propellant fabrication on Mars

Shah Saud Alam,[1] Christopher Depcik,[1,4,*] Sindhu Preetham Burugupally,[2] Jared Hobeck,[3] and Ethan McDaniel[2]

SUMMARY

***In-situ* resource utilization (ISRU) to refuel rockets on Mars will become critical in the future. The current effort presents a thorough feasibility analysis of a scalable, Matlab-based, integrated ISRU framework from the standpoint of the second law of thermodynamics. The ISRU model is based on existing technology that can utilize Martian resources (regolith and atmosphere) to produce rocket propellants. Model simulations show that the system analysis is theoretically consistent with a positive entropy generation, and the achievable mass flow rates of liquid methane and liquid oxygen can potentially meet the 16-month rocket refueling deadline (on Mars) as desired by the National Aeronautics and Space Administration. However, the model is sensitive to liquid oxygen storage temperatures, and lower temperatures are necessary to minimize compressor work. This proof-of-concept model can open avenues for further experimental evaluation of the system to achieve a higher technology readiness level.**

INTRODUCTION

Riding on the success of several Mars missions over the last few decades, the National Aeronautics and Space Administration (NASA) and the Space Exploration Technologies Corporation (SpaceX) are working collectively across multiple disciplines in a quest to colonize Mars by the 2030s (Chen et al., 2020; Liu et al., 2021; Shishko et al., 2017). Sending humans to Mars would necessitate return missions, and current rocket technology is incapable of supporting this outcome (Johnson et al., 2018). Rockets usually make one-way trips to space and are largely limited by their weight, which is mostly liquid propellant (up to 80 wt%) (Ash et al., 1978). It is estimated that each kilogram of *useful* technology sent to Mars requires 7–11 kg of mass launched from Earth and translates to 5.6–8.8 kg of propellant needed per kilogram of material (Johnson et al., 2018). If transporting propellant from Earth to Mars to set up a local fuel depot, *gear ratios* become an important consideration during mission design (Leucht, 2018) and estimates show that Mars requires a gear ratio of 226:1 (Sanders et al., 2015). In other words, 226 kg of propellant is required to have 1 kg of propellant on Mars.

The transportation of critical resources to space or other planets is cost-prohibitive with water costing $20,000 per liter to send into space (Zacny et al., 2012). Recently, SpaceX has invented reusable rockets (*Starship*) to alleviate this problem (Palmer, 2021; Sheehan, 2021). Although reusing the rockets lowers mission costs significantly, it still suffers from the limitation posed by the large propellant payload required for the trip to Mars. A potential solution arises in the form of refueling rockets on planets and moons, with some studies showing that rocket refueling on Mars would reduce the terrestrial propellant use by 30% (Landis and Linne, 2001). Exploiting local Martian resources, also known as *in-situ* resource utilization (ISRU), to produce rocket propellants (aka *in-situ* propellant production or ISPP) becomes critical for future missions that encompass both return missions and extended deep-space missions.

NASA has conducted several ISRU programs for Mars in the past to potentially lower the interplanetary logistical costs (Wang et al., 2011), with the latest being the Mars Oxygen ISRU Experiment (MOXIE) onboard the Curiosity rover (Starr and Muscatello, 2020). Although NASA developed ISRU technology commercially via its Small Business Innovative Research program, most of this technology was developed at a low technology readiness level (TRL) as shown in Figure 1. Viewing the importance of Mars ISPP for future missions, NASA has actively accelerated research in this direction since 2016 to develop TRL6 (and higher) technologies to proceed to mission design by the next decade (Starr and Muscatello, 2020). There is an opportunity to develop an ISPP framework for Mars that encompasses several critical aspects

[1]Department of Mechanical Engineering, University of Kansas, Lawrence, KS 66045, USA

[2]Department of Mechanical Engineering, Wichita State University, Wichita, KS 67260, USA

[3]Alan Levin Department of Mechanical and Nuclear Engineering, Kansas State University, Manhattan, KS 66506, USA

[4]Lead contact

*Correspondence: depcik@ku.edu

https://doi.org/10.1016/j.isci.2022.104323

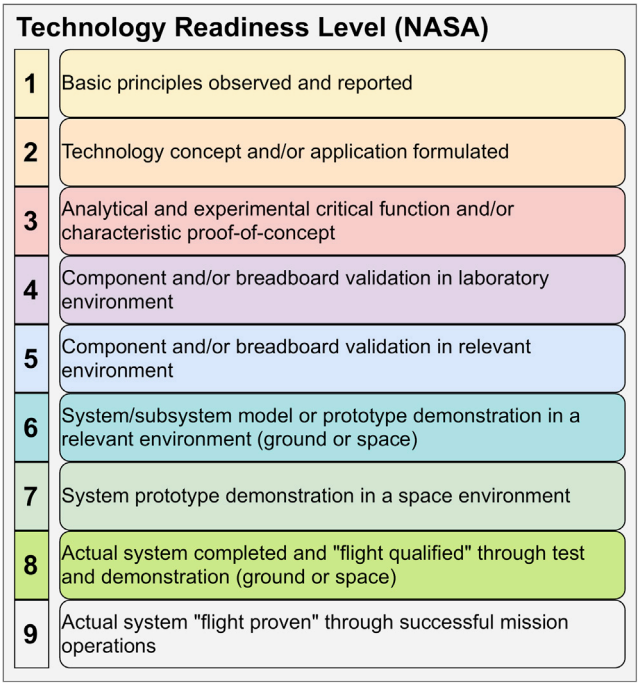

Figure 1. Technology readiness levels as specified by the National Aeronautics and Space Administration (NASA, 2012)

of the technology. Before developing and validating such a framework, it is important to finalize a fuel from among the commonly used rocket fuels that can be fabricated *in situ*.

Current rocket propellants range from hydrogen to ethanol to kerosene depending on their carbon chain length. Liquid hydrogen-oxygen, carbon monoxide-oxygen, and methane-oxygen are considered the most common rocket propellants (Ash et al., 1978). Table 1 shows a normalized comparison of the cryogenic and propulsive characteristics of these three fuels to facilitate the selection of the better fuel. It is readily clear from Table 1 that, although hydrogen offers superior rocket thrust compared to carbon monoxide and methane, it has a significantly lower boiling temperature (20.4 K). Its liquefaction and storage over a long journey are problematic due to the high cryogenic power consumption. Comparatively, carbon monoxide requires the lowest energy for liquefaction but at the same time, it suffers from the lowest estimated specific impulse among the three fuels. In contrast, the lower liquefaction work required for methane compared with hydrogen and a relatively superior thrust performance compared with carbon monoxide makes methane typically the fuel of choice for reusable rockets (Ash et al., 1978; Clapp, 1991; Linne et al., 1990; Sullivan et al., 1995).

The Martian environment favors methane formation over hydrogen and carbon monoxide and is thermodynamically superior to Earth due to the following reasons. First, Mars's carbon-dioxide-rich atmosphere (≈94.90 vol% [Franz et al., 2017]) and approximately 10 wt% water in the Martian regolith (Zacny et al., 2012) provide the critical ingredients for the production of methane. Secondly, the recorded average ambient temperature on Mars ranges from 210 K to 230 K (Starr and Muscatello, 2020), which effectively turns the Martian atmosphere into a comparatively better heat sink that can assist power generation and refrigeration systems (Ash et al., 1978). Finally, a diurnal amplitude of about 60 K in the daily ambient temperature can significantly improve the performance of refrigeration systems that require intermittent operation (Ash et al., 1978). Based on these characteristics and readily available technology on Earth, Mars offers a significant opportunity for methane-based ISPP. NASA hopes to set up an *in-situ* propellant production on Mars that can leverage local conditions to refuel 7 metric tons of liquid methane and 22 metric tons of liquid oxygen in 16 months (Leucht, 2018). In comparison, the SpaceX Starships that could carry humans to Mars and back would need to be refueled with 267 metric tons of liquid methane and 933 metric tons of liquid oxygen (Heldmann et al., 2021).

Table 1. Normalized cryogenic requirements and propulsive characteristics of the three most popular rocket fuels—hydrogen, carbon monoxide, and methane

Fuel	Normalized propellant liquefaction work [-]	Liquefaction temperature (K)[a]	Normalized specific impulse [-][b]
Hydrogen	3.609	20.4	1.646
Carbon monoxide	1.056	81.6	1.000
Methane	1.000	111.4	1.319

See (Ash et al., 1978).
[a]Pressure: 1.013 bar.
[b]Chamber pressure: 27.6 bar, area expansion ratio: 80:1, atmospheric pressure: 6.6 mbar, a specific impulse of 89% equilibrium value.

On Earth, the Sabatier reaction can play an important role in the production of methane. It is a thermodynamically favored reaction of carbon dioxide and hydrogen over a suitable catalyst to produce methane along with heat ($\Delta H = -165$ kJ/mol) at a relatively low temperature (Falbo et al., 2019; Malara et al., 2020; Rönsch et al., 2016; Stangeland et al., 2017). Over the last century, the Sabatier reaction (commonly known as the hydrogenation of carbon dioxide or methanation) has become an important reaction from the standpoint of catalysis, biology, surface science, nanoscience, and environmental science (Wang et al., 2011). For Mars ISPP, the use of the Sabatier process and other supporting technologies including atmospheric carbon dioxide capture, water mining, and water electrolysis was first proposed by Ash et al. (1978), in 1978. Their findings were significantly detailed from the standpoint of mission design. Later, in 1997, Reddig and MacKnight devised an integrated system that was capable of producing 0.7 kg/day of liquid methane from atmospheric carbon dioxide via a ruthenium-catalyzed Sabatier reaction (Reddig and MacKnight, 1997). They validated their methodology with a thermodynamic analysis of the ISPP system using black-box process modeling software. A few years later, Salerno and Kittel analyzed another integrated ISPP system and emphasized the transport of hydrogen from Earth to Mars as a seed for kick-starting the Sabatier reaction to produce methane (Salerno and Kittel, 1999). In 2002, Zubrin et al. investigated the Sabatier reaction and water electrolysis to develop an end-to-end Mars ISPP system (Zubrin et al., 2002). A recent study by Starr and Muscatello mentions that SpaceX has planned to employ the Sabatier reaction on Mars for ISPP (Starr and Muscatello, 2020). They indicate that a practical ISPP is possible within the bounds of the existing technology although scaled up (approx. 2×) in capacity from existing laboratory models.

Although these efforts indicate the importance of the Sabatier reaction for Mars ISPP, none provide detailed specifics on the pertinent catalytic parameters, such as the catalyst used and its activity, methane selectivity, and carbon dioxide conversion, that are critical for process design. Furthermore, black-box software should not be trusted for system design, especially when human lives are at stake (Alam and Depcik, 2019). There is a need to dive deeper into the fundamentals and validate an ISPP system based on the laws of thermodynamics. The processes must be carefully designed with suitable catalysts and the important parameters must be incorporated into the thermodynamic analysis for a proof of concept. Thus, this paper focuses on a detailed ISRU framework based on the block diagram in Figure 2 to produce methane and oxygen on Mars using existing technology within 16 months to meet the NASA deadline. The ISRU system indicated can be constructed and validated today on Earth using available hardware with the laws of thermodynamics employed to validate the concept providing a proof-of-concept at TRL 3.

In the proposed system, water is mined from the Martian regolith, condensed, and stored as a liquid. Then, water is electrolyzed to retrieve hydrogen and oxygen. Although oxygen is sent to a liquefaction subsystem, the hydrogen is passed into a Sabatier reactor. In parallel, atmospheric carbon dioxide is captured and stored as a liquid before being reacted with hydrogen to produce a gaseous mixture comprising methane, carbon dioxide, carbon monoxide, hydrogen, and water vapor. This mixture is passed through a water recovery system to condense and recycle water. The exiting *dry* mixture of gases flows through a gas separation chamber where pressure swing adsorption (PSA) is employed to capture and recycle carbon dioxide and hydrogen gases while allowing methane to pass through to a methane liquefaction and storage system.

A detailed version of such a framework is presented in Figure 3. The starting points for the analysis are the temperatures and pressures of the water mining and atmospheric carbon dioxide capture blocks.

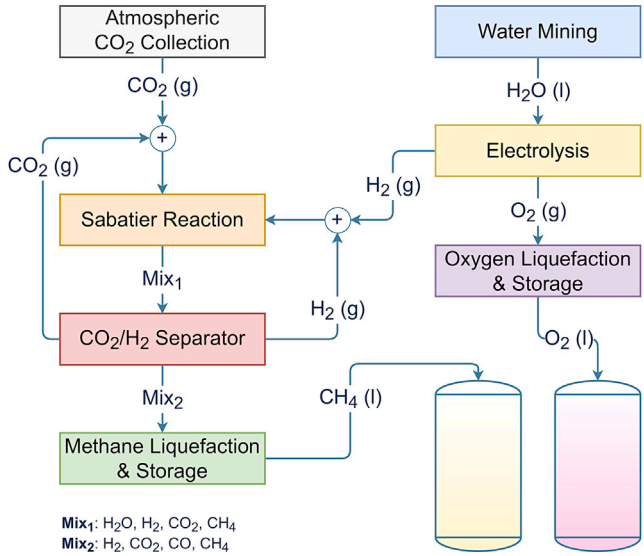

Figure 2. Basic block diagram of the *in-situ* methane and oxygen production on Mars

Knowledge of the Sabatier reaction specifics, as well as the state variables necessary to maximize the yield of liquid methane and oxygen, helps in the completion of the analysis. A Martian atmosphere temperature of 210 K was used for heat transfer purposes. This choice was based on the experimental work for atmospheric CO_2 collection. An analysis of Spirit and Opportunity rover data finds that the average temperature can vary from about 197 K to 280 K over the seasons (Spanovich et al., 2006). A small sensitivity study concerning oxygen liquefaction is described later to illustrate the influence of storage temperature on system performance.

Water mining

Water mining involves the extraction of water from the icy Martian regolith and its subsequent storage. Although there are a few experimental and simulation findings available in the literature (Adan-Plaza et al., 1998; England, 2001; Linne and Kleinhenz, 2016; Wiens et al., 2001; Zacny et al., 2012), simulation-based studies often show a significantly larger power consumption compared with experimental findings (e.g., 350 kW consumption to produce 0.76 kg of water per hour [England, 2001]); this is primarily due to a lack of appropriate assumptions and that is why they were not considered for the current effort. The experimental works of Zacny et al. (2012) and Linne and Kleinhenz (2016) were shortlisted due to their real-world results and on close examination, the efforts of Zacny et al. were used due to their comparatively better results.

Zacny et al. mention that the hardness of the icy soil on Mars increases with saturation (ice content in the soil) and can be 2–3× harder than concrete and sandstone (Zacny et al., 2012). Therefore, the rate of water extraction on Mars is limited by the hardness of the regolith. Space and weight limitations necessitate the use of integrated mobile mining and water extraction systems (aka Mobile *In-Situ* Water Extractor or MISWE). Onboard the logistically beneficial MISWE, the mined ice can be heated for sublimation. As the vapor content grows inside the reactor, convection becomes the dominant mode of heat transfer that further promotes the sublimation process. Because the reactor pressure grows proportional to the vapor content, a one-way valve (check valve) becomes essential to keep the reactor at safe operating pressures. With this valve, the water vapor flows to a storage canister where the stream pressure drops significantly, and the water vapor condenses quickly into liquid water. Their experiments show that MISWE consumes 34 Watts of energy over 40 min, primarily for heat generation, and achieves a 91.54% efficiency at 12 wt% ice composition. The current model employs Zacny's projection to recover 200 g of water every 40 min at the expense of 340 Watts of heat. Validation of the simulation results is done by ensuring that the mined water is in a liquid state.

Although the water at the North pole of Mars might be 95% pure (Grima et al., 2009), no resources were found that indicate the respective purity of water within the regolith. As stated by Pickett et al. (2020) and Heldmann et al. (2021), water recovered *in situ* will likely require a purification process to remove

Table 2. Temperature and pressure at the different states and corresponding mass flow rates of the different gases

			mdot (g/s)											
State	T (K)	P (Pa)	H_2O (g)	H_2 (g)	O_2 (g)	Ar (g)	CO_2 (g)	CO (g)	N_2 (g)	H_2O (L)	CH_4 (g)	CO_2 (L)	O_2 (L)	CH_4 (L)
1	273.15	1.352×10^5	0	0	0	0	0	0	0	0.083	0	0	0	0
2	273.15	3.485×10^6	0	0	0	0	0	0	0	0	0	5.556×10^{-3}	0	0
3	210.00	6.100×10^2	0	0	1.481×10^{-5}	2.211×10^{-4}	1.111×10^{-2}	5.566×10^{-6}	2.079×10^{-4}	0	0	0	0	0
4	210.00	6.100×10^2	0	0	1.481×10^{-5}	2.211×10^{-4}	5.556×10^{-3}	5.566×10^{-6}	2.079×10^{-4}	0	0	0	0	0
5	273.15	1.352×10^5	0	0	0	0	0	0	0	1.100	0	0	0	0
6	273.15	1.352×10^5	0	0	0.977	0	0	0	0	0	0	0	0	0
7	273.15	1.352×10^5	0	0.123	0	0	0	0	0	0	0	0	0	0
8	93.04	1.352×10^5	0	0	0	0	0	0	0	0	0	0	0.977	0
9	211.01	1.352×10^5	0	0	61.364	0	0	0	0	0	0	0	0	0
10	1293.05	4.275×10^7	0	0	61.364	0	0	0	0	0	0	0	0	0
11	210.00	4.275×10^7	0	0	61.364	0	0	0	0	0	0	0	0	0
12	93.04	1.352×10^5	0	0	61.364	0	0	0	0	0	0	0	0	0
13	93.04	1.352×10^5	0	0	60.387	0	0	0	0	0	0	0	0	0
14	210.00	1.352×10^5	0	0	60.387	0	0	0	0	0	0	0	0	0
15	273.15	3.485×10^6	0	0	0	0	0.523	0	0	0	0	0	0	0
16	583.15	1.352×10^5	0	0	0	0	0.838	0	0	0	0	0	0	0
17	583.15	1.352×10^5	0	0.154	0	0	0	0	0	0	0	0	0	0
18	583.15	1.352×10^5	0.378	0.035	0	0	0.336	1.475×10^{-3}	0	0	0.168	0	0	0
19	273.15	1.352×10^5	0	0	0	0	0	0	0	0.378	0	0	0	0
20	273.15	1.352×10^5	0	0.035	0	0	0.336	1.475×10^{-3}	0	0	0.168	0	0	0
21	601.12	1.824×10^6	0	0.035	0	0	0.336	1.475×10^{-3}	0	0	0.168	0	0	0
22	294.15	1.824×10^6	0	0.035	0	0	0.336	1.475×10^{-3}	0	0	0.168	0	0	0
23	294.15	1.824×10^6	0	0.031	0	0	0	0	0	0	0	0	0	0
24	294.15	1.013×10^5	0	0	0	0	0.315	0	0	0	0	0	0	0
25	294.15	1.013×10^5	0	4.523×10^{-3}	0	0	0.020	1.475×10^{-3}	0	0	0.168	0	0	0
26	294.65	1.352×10^5	0	0.031	0	0	0	0	0	0	0	0	0	0
27	706.93	3.485×10^6	0	0	0	0	0.315	0	0	0	0	0	0	0
28	719.33	3.485×10^6	0	4.523×10^{-3}	0	0	0.020	1.475×10^{-3}	0	0	0.168	0	0	0
29	273.15	3.485×10^6	0	4.523×10^{-3}	0	0	0	1.475×10^{-3}	0	0	0.168	0	0	0
30	273.15	3.485×10^6	0	0	0	0	0	0	0	0	0	0.020	0	0
31	372.98	9.136×10^6	0	4.523×10^{-3}	0	0	0	1.475×10^{-3}	0	0	0.168	0	0	0
32	210.00	9.136×10^6	0	4.523×10^{-3}	0	0	0	1.475×10^{-3}	0	0	0.168	0	0	0
33	112.60	1.333×10^5	0	4.523×10^{-3}	0	0	0	1.475×10^{-3}	0	0	0.168	0	0	0
34	112.60	1.093×10^5	0	0	0	0	0	0	0	0	0	0	0	0.168
35	112.60	2.397×10^4	0	4.523×10^{-3}	0	0	0	1.475×10^{-3}	0	0	0	0	0	0

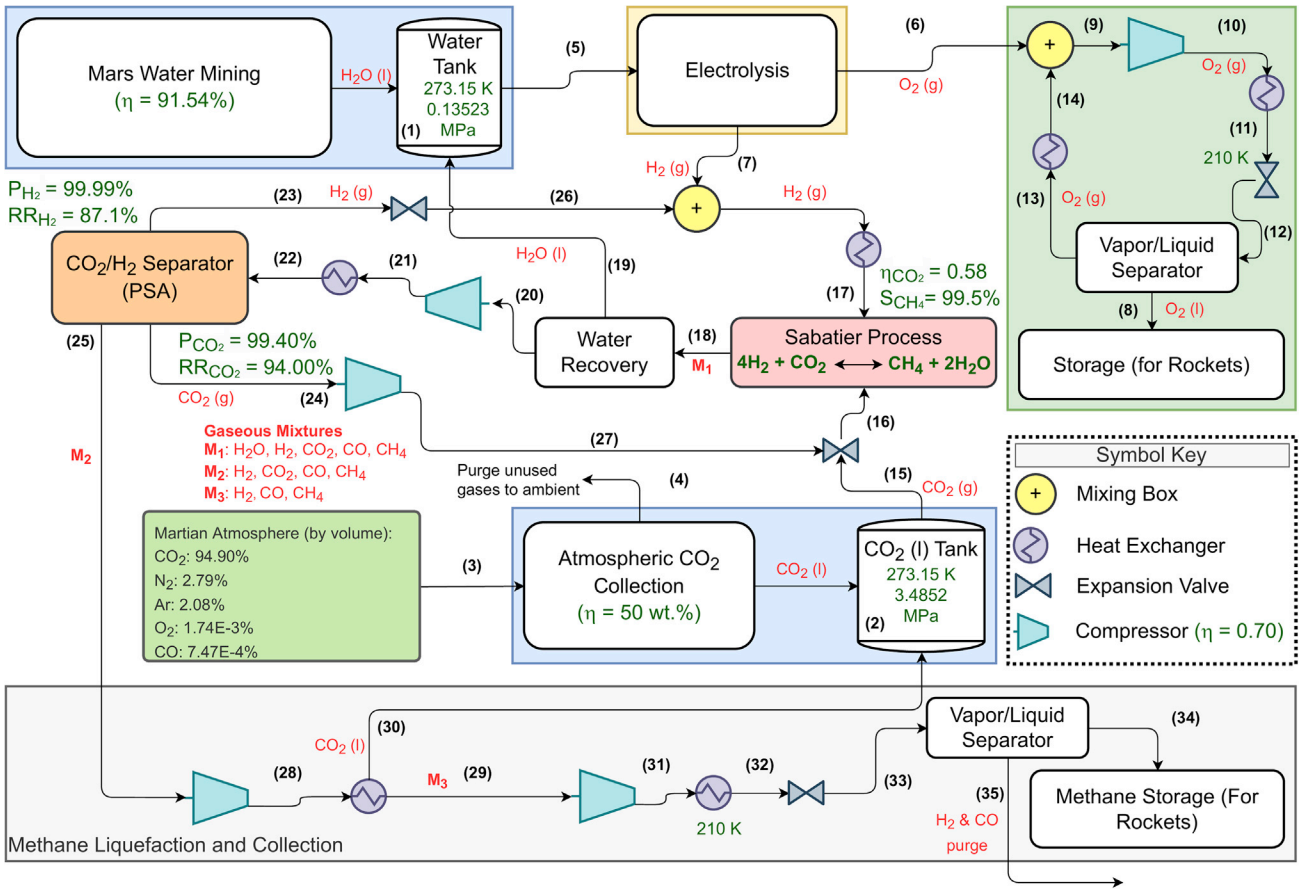

Figure 3. Complete system schematic with states

The Martian atmospheric composition and the state variables for the atmospheric carbon dioxide capture and water mining serve as the starting points of the analysis. Corresponding variables and flow rates for each state are listed in Table 2.

contaminants and biological material. The respective material and energy resources needed for this purification process are not included in this effort and are left to a future study.

Electrolysis

The stored water from the water mining subsystem is electrolyzed by applying a direct current that breaks the water molecule into hydrogen and water as shown by Equation (1):

$$2\,H_2O \rightarrow 2\,H_2 + O_2 \qquad \text{(Equation 1)}$$

where pure hydrogen and oxygen emanate from the cathode and anode, respectively, at the same pressure and temperature (Todd et al., 2014).

The hydrogen and oxygen flow rates are determined by applying a mass balance on Equation (1) and using the water mining exit flow rates. Due to the application of electric current during electrolysis, the energy equation is modified to include electrical energy along with other usual assumptions mentioned prior. This determines the thermoneutral cell potential, E_{tcp}, (in volts) as

$$E_{tcp} = \frac{\dot{W}_{CV} - \dot{Q}_{CV}}{n \bullet F} = \frac{\dot{n}_{H_2O} \bullet \overline{h}_{H_2O} - \dot{n}_{H_2} \bullet \overline{h}_{H_2} - \dot{n}_{O_2} \bullet \overline{h}_{O_2}}{n \bullet F} \quad [\text{Volts}] \qquad \text{(Equation 2)}$$

where n is equal to 2 for water and F is the Faraday constant and is equal to 96,485.33 A•s/mol. The reversible cell potential (E_{rev}) method is comparatively better at determining the cell potential required for

electrolysis, as it invokes the second law in the calculations by assuming that the environment provides the necessary $T\Delta S$ term at a temperature T, thus, delivering more accurate results compared with the E_{tcp} method:

$$E_{rev} = \frac{\dot{W}_{rev}}{n \bullet F} = \frac{\dot{n}_{H_2O} \bullet \overline{g}_{H_2O} - \dot{n}_{H_2} \bullet \overline{g}_{H_2} - \dot{n}_{O_2} \bullet \overline{g}_{O_2}}{n \bullet F} \quad [\text{Volts}] \qquad \text{(Equation 3)}$$

Employing Equation (3) helps in the determination of the energy consumption during water electrolysis to fully electrolyze the incoming water stream before feeding the exiting hydrogen and oxygen streams to the methanation and liquefaction systems, respectively. It is important to note that even with an estimated energy efficiency of 70% (Yan et al., 2019), this will likely underestimate the power requirements for electrolysis in comparison to commercially available systems (Ursua et al., 2012). The choice here was made to synchronize with the water mining data from Zacny et al., and future work should investigate commercial electrolyzers and their operation under the thermodynamic conditions provided. This might require adjusting the water tank conditions for optimal production of hydrogen at a minimum of energy.

Atmospheric carbon dioxide capture

Atmospheric carbon dioxide can be collected from the atmosphere via the Integrated Cryogenic Extraction of Carbon dioxide and Utilization By Expansion (ICE CUBE) technology that was originally designed, developed, and implemented by the Lockheed Martin Space Systems Corporation (LMSSC) (Sanders et al., 2014). The choice of this technology serves two purposes: feedstock for the Sabatier reaction and oxygen production for human exploration after CO_2 conversion. If rocket fuel is the only desired outcome, it is possible to utilize solution-diffusion gas membranes or other technologies for CO_2 separation (Muscatello et al., 2011); this would result in some impurities from the Martian atmosphere, making their way into the Sabatier reaction; however, as these are mostly the inert compounds of nitrogen and argon, they should not affect reactor effectiveness significantly.

The ICE CUBE method involves the freezing/heating of carbon dioxide and operates under two modes—carbon dioxide collection mode and pressurized carbon dioxide delivery mode. In the collection mode, either filtered or unfiltered Martian atmosphere is inducted into the system and cooled to the triple point of carbon dioxide at Mars' pressure (150 K) to freeze carbon dioxide while rejecting the other constituent gases. During this process, water vapor may not be ejected from the system completely. At a 273.15 K thermal interface and a Mars atmospheric temperature of 210 K, the cryocooler delivers 4 W (W) of cooling from an average power draw of 40 W. Assuming an operational efficiency $\geq$50%, Sanders et al. (2014) showed that the ICE CUBE is capable of delivering approximately 0.16 kg of carbon dioxide per operation cycle (8 h) at a capture rate of 20 g/h. Sanders et al. demonstrated this method to be a simple, durable, and mass- and power-efficient TRL6 method. This ICE CUBE system was sized to the payload requirements of the 2020 Mars rover mission designed by NASA, and the weight of the final system was not to exceed the 15-kg limit imposed.

Sabatier process for methane and water production

Methane is produced from the reaction of carbon dioxide and hydrogen in a process known as the Sabatier reaction or methanation of carbon dioxide. This reaction occurs over a suitable catalyst, preferably, nickel, or ruthenium, via the following exothermic reaction (Guerra et al., 2018):

$$4H_2 + CO_2 \rightarrow CH_4 + 2H_2O \; [\Delta H^{\circ} = -165 \text{ kJ/mol}] \qquad \text{(Equation 4)}$$

Because catalysts get deactivated by chlorine, tar particles, ammonia, sulfur compounds, alkalis, and carbon deposition (aka coking) (Rönsch et al., 2016), it is important to select a suitable catalyst for the Sabatier reaction. Catalysts with good metal dispersion characteristics and resistance to deactivation as well as good anti-sintering properties are preferred. In addition, good catalysts should deliver high carbon dioxide conversion and a greater methane yield along with enhanced carbon monoxide inhibition (Frontera et al., 2017; Su et al., 2016). Two of the commonly employed catalysts that meet the selection criteria for the Sabatier process are nickel (Ni) and ruthenium (Ru) (Garbarino et al., 2015; Rönsch et al., 2016; Stangeland et al., 2017).

Unhindered operation of the Sabatier reaction on Mars requires a catalyst that is easily activated and shows high activity and methane selectivity along with good resistance to deactivation by sintering, fouling, and

coking. In this regard, Ru-based catalysts exhibit superior performance compared with Ni-based catalysts at similar operating conditions and are more stable over a wider range of operating conditions (Falbo et al., 2019; Frontera et al., 2017; Garbarino et al., 2015; Moioli and Züttel, 2020; Rönsch et al., 2016; Su et al., 2016). Because they are activated at 473.15 K (100 K lower than Ni-based catalysts), Ru-based catalysts have higher selectivity toward methane (>95%) (Moioli and Züttel, 2020). Unlike Ni-based catalysts, carbon monoxide production over Ru-based catalysts is negligible (Falbo et al., 2019; Frontera et al., 2017; Garbarino et al., 2015). At low pressures, these catalysts can also convert carbon monoxide to methane, further lowering carbon monoxide concentration in the effluent (Falbo et al., 2019).

Although Ru-based catalysts look promising compared with nickel-based versions, they do have limitations. Ruthenium is 120× more expensive than nickel (on a mass basis) and is cost-prohibitive for large-scale operations (Moioli and Züttel, 2020; Rönsch et al., 2016). Ru-based catalysts can deactivate either from sintering at high temperatures or from the formation of ruthenium-carbonyls at low temperatures (Falbo et al., 2019). Such deactivation is rare compared with Ni-based catalysts, and even in the case of deactivation, Ru-based catalyst sites can be readily reactivated by increasing the operating temperature and treating the catalyst sites with hydrogen (Falbo et al., 2019).

To sum up, Ru-based catalysts offer more activity, stability, and resistance to deactivation at a higher cost. Because a sustained and reliable operation of all systems on Mars is paramount for the success of the entire operation, the monetary burden can be overlooked while selecting Ru-based catalysts for the Sabatier process on Mars. As a result, the work of Falbo et al. concerning the use of a Ru/Al_2O_3 catalyst at 583.15 K under atmospheric pressure with a 58% carbon dioxide conversion efficiency and a 99.5% selectivity toward methane was chosen for the current effort (Falbo et al., 2019).

The operation of the Sabatier system at atmospheric pressure minimizes the energy expenditure associated with raising inlet stream pressures while operating at a similar pressure to electrolysis. The inlet hydrogen and carbon dioxide streams are heated to the system temperature of 583.15 K before entering the Sabatier system. Based on the specifics from Falbo et al. (2019), an iterative analysis in Matlab R2021 determines the mass flow rates of the gaseous mixture and assesses the thermodynamic performance of the system. The product gases comprising methane, water, carbon dioxide, carbon monoxide, and hydrogen exit the system. To maximize cycle efficiency, the product gases are fed into a condenser to recover water for reuse in the electrolysis subsystem. The emerging *dry* gases are fed into a pressure swing adsorption (PSA) system to separate the constituent gases before sending them for further enrichment or storage. Because water molecules deactivate the PSA adsorbent (Wiheeb et al., 2015), the removal of water from the feed enhances the efficiency of the PSA process.

Carbon dioxide and hydrogen separation (pressure swing adsorption)

Pressure swing adsorption is a simple and energy-efficient process for gas separation and purification that can work in tandem with the Sabatier process to produce carbon dioxide, hydrogen, and methane on Mars (Park et al., 2017; Sircar, 2002; Sircar and Golden, 2000; Voldsund et al., 2016; Wiessner, 1988; Wiheeb et al., 2015; Zhu et al., 2019). Since the 1980s, PSA has been widely used for the separation of hydrogen from gaseous streams, and its subsequent purification can sometimes exceed 99.99% (Voldsund et al., 2016). In the case of carbon dioxide, PSA presents one of the biggest challenges, both technically and economically, due to the stability of the carbon dioxide molecule. Because the carbon dioxide molecule has a large permanent quadrupole moment, it strongly binds to the adsorbent at low partial pressures and makes its desorption difficult (Sircar and Golden, 2000). Common adsorbents for carbon dioxide are zeolites and activated carbon, which show greater efficiency in removing carbon dioxide from a stream (Sircar and Golden, 2000). They require system temperatures below 373.15 K for optimal performance as their performance deteriorates with increasing temperature (Wiheeb et al., 2015).

Due to their affinity toward carbon dioxide and hydrogen, both zeolites and activated carbon can be employed in a specially designed multibed PSA reactor for the simultaneous production of pure carbon dioxide and hydrogen. Sircar and Golden (Sircar and Golden (2000) show that these systems are capable of producing a primary hydrogen product at a purity of 99.999% and a recovery rate of 87.1% along with a secondary carbon dioxide product at a purity of 99.4% and a recovery rate of 94% at operating pressure and temperature of 18 atm (1.824 MPa) and 294.15 K, respectively. In these multibed systems, the feed gas is first passed over activated carbon to selectively remove carbon dioxide and any remaining water. The

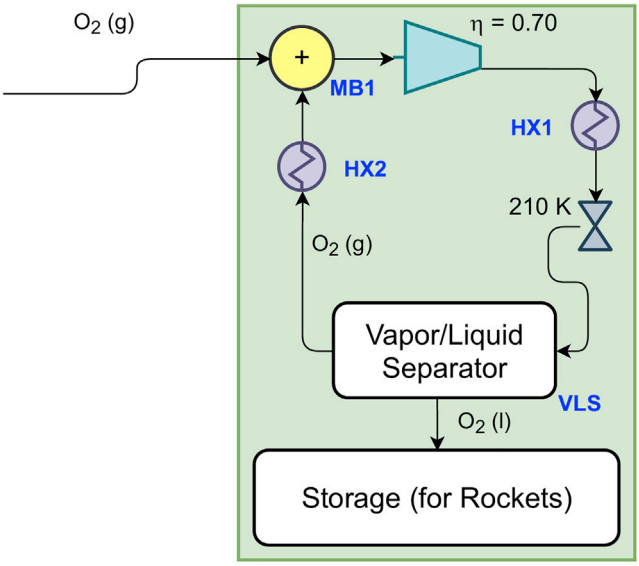

Figure 4. Schematic of the oxygen liquefaction subsystem

exiting stream is passed over zeolites to remove the remaining carbon dioxide along with methane and carbon monoxide from hydrogen. This multibed PSA approach is ideal for deployment on Mars and used here for the separation and purification of carbon dioxide, methane, and hydrogen.

Oxygen liquefaction and storage

Liquefied oxygen (or LO_x) is commonly used as a cryogenic liquid oxidizer propellant for spacecraft applications; this is achieved via the Linde cycle, which delivers liquefied gases at higher temperatures and pressures via cascaded compression stages (Johnson et al., 2018), and a representative system is included in Figure 4.

During the oxygen liquefaction process, the gaseous oxygen exiting the electrolysis subsystem goes through a mixing box (MB1) where its pressure is held constant while its temperature changes due to mixing. A compressor operating at an assumed isentropic efficiency of 70% compresses oxygen to a pressure where the enthalpy of oxygen is minimum at Martian night temperature (210 K) after the use of a heat exchanger exposed to the ambient (HX1). This pressure is determined from the oxygen's *p-h* diagram (Figure 5) with Matlab's *fminsearch* and REFPROP10. The choice of a minimum enthalpy follows from the use of a valve following this process. Subsequently, assuming a constant enthalpy valve process as shown in Figure 5 indicates that this will result in the smallest value of quality after the valve as the working fluid drops into the two-phase region and provides the greatest amount of liquid O_2. A vapor-liquid separator (VLS) is employed to separate the gaseous oxygen from its liquid phase via gravity. The recycled oxygen exiting the VLS is fed into another heat exchanger (HX2) exposed to the Martian atmosphere that raises the stream temperature before entering MB1; this ensures that gas enters the compressor, which prevents any accidental damage. An iterative analysis was conducted in Matlab to simulate steady-state operation.

Methane liquefaction and storage

Methane liquefaction is not as straightforward as oxygen liquefaction. The gas mixture exiting the PSA subsystem comprises carbon dioxide, hydrogen, and carbon monoxide along with methane. A closer look at their properties reveals that methane liquefies at a temperature below the solidification temperature of carbon dioxide. solid carbon dioxide in the subsystem could potentially be detrimental, it is important to liquefy and remove it from this gas mixture before proceeding with methane liquefaction. As shown in Figure 6, a compressor with an isentropic efficiency of 70% is employed to raise the gas mixture pressure to match the pressure of the liquid carbon dioxide tank. The hot gases exiting the compressor are passed through a heat exchanger (HX3) where they cool down to the carbon dioxide tank temperature at constant pressure. The liquid carbon dioxide is then separated from the rest of the gases and collected.

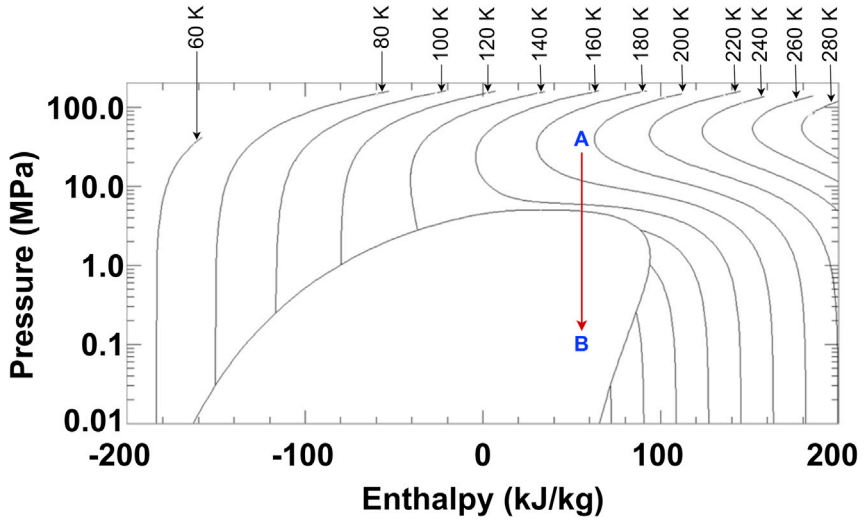

Figure 5. Pressure-enthalpy diagram for oxygen (from REFPROP10) showing the pressure at the lowest enthalpy before going through a valve (A: valve inlet, B: valve outlet)

Unlike the oxygen liquefaction system where a single gas was being liquefied, the methane liquefaction system has to consider a gaseous mixture. Dalton's law of partial pressures becomes applicable in such a scenario that requires analyzing the subsystem in *reverse*; this includes first assuming a methane quality of 0 at the standard Earth methane liquefaction temperature of 111.1 K (Prydz and Goodwin, 1972) exiting the vapor/liquid separator and entering the methane storage tank, which provides the pressure exiting the valve after accounting for Dalton's law. Subsequently, Matlab's *fminsearch* function was utilized to find a pressure at 210 K that balanced the valve energy equation. If the difference in enthalpies was greater than 1×10^{-5}, the methane liquefaction temperature was increased by 0.1 K, and the process was repeated. This resulted in the lowest temperature of methane liquid and the greatest density that would minimize the methane storage tank size. Because the heat exchange is assumed to occur at constant pressure in HX4, the pressure at its outlet also becomes the exit pressure at the compressor preceding it, and the governing equations were used on the compressor last. It was assumed that the gases (hydrogen and carbon dioxide) are purged into the ambient Martian atmosphere.

RESULTS

Before analyzing the entire system, it is important to mention that heat balance optimization was not accomplished. It is possible to collocate devices with one device rejecting heat and the other absorbing that heat. However, this system optimization was left to future efforts.

The detailed thermodynamic assessment of the overall system begins with water mining where it is determined that ice is extracted at a rate of 0.083 g/s from the Martian regolith at 223.15 K and then sublimed in a reactor operating at 611.73 Pa and 273.15 K. A preliminary calculation based on the energies needed per gram of water extracted and sublimed shows that this system is 83.11% efficient (η_{system}).

Water is then electrolyzed to produce oxygen and hydrogen that are fed into the oxygen liquefaction subsystem and a mixing box (eventually, leading to the Sabatier subsystem), respectively. Assuming a water feed of 1.1 g/s to the electrolysis chamber, oxygen and hydrogen flow rates are observed to be 0.98 g/s and 0.12 g/s, respectively. The water flow rate depends on the desired liquid methane flow rate and can vary as necessitated by the design requirements. A potential of 1.25 V needs to be maintained between the electrodes to break the water molecule into its respective constituent molecules. Factoring in the flow rate information reveals that approximately 21.13 kW of electrical energy is consumed during electrolysis. Both oxygen and hydrogen exit the electrolysis chamber at 273.15 K and 0.13523 MPa.

Oxygen is then liquefied for storage while leveraging Martian nighttime temperatures to minimize power consumption. Using *fminsearch* in Matlab, the pressure corresponding to the lowest enthalpy of oxygen at Martian nighttime temperature (210 K) was found to be 42.75 MPa. The compressor employed to raise the

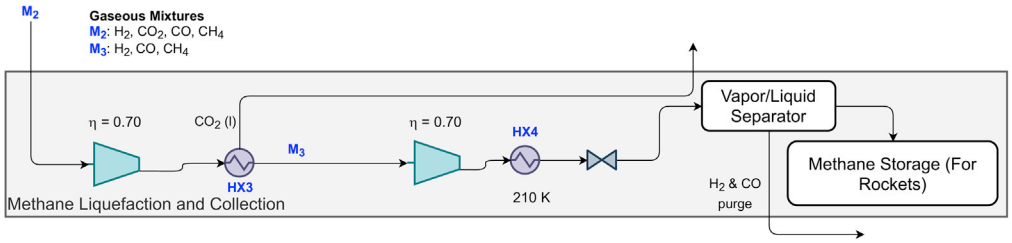

Figure 6. Schematic of the methane liquefaction system

pressure of the incoming gases to this value consumed 69.79 kW. Subsequently, a heat exchanger and expansion valve arrangement successively cooled the gas down to its liquefaction temperature. First, the heat exchanger rejects 76.69 kW of heat to the ambient Martian atmosphere (at night) and cools the gas to 210 K. Then, gas expansion through the valve further reduces its temperature to 93.04 K while also lowering its pressure to 0.13523 MPa. Because cryogenic methods were not employed, the fluid entering the vapor-liquid separator is 93.33% vapor and necessitates oxygen recycling to achieve higher flow rates of liquid oxygen. As the gaseous oxygen exiting the vapor-liquid separator is at a lower temperature compared with fresh oxygen, another heat exchanger is employed to raise its temperature to 210 K before mixing. The calculations show that this heat exchanger adds 6.55 kW of heat to the passing oxygen by leveraging the temperature delta between the fluid and ambient temperatures. Liquid oxygen is collected and stored in a tank at 93.04 K and 0.13523 MPa after successive recycling.

Meanwhile, carbon dioxide is captured from the atmosphere at the rate of 5.56 mg/s (collection rate: 0.052 L/s), assuming an effective capture efficiency of 50%. The recovered carbon dioxide is purified and compressed to 91.5 kPa at a compression ratio >150:1 before liquefaction. The power consumption during compression averages 50 W; however, the peak power draw can reach 60 W under typical operating conditions. In addition, employing the ICE CUBE system to liquefy pure carbon dioxide via the miniature cryocooler results in an effective compression of 5000:1 without the use of additional compressor(s) (Sanders et al., 2014). The liquefied carbon dioxide is then stored in a tank at 3.49 MPa and 273.15 K. The subsystem consumes 2.5 W-hr of energy per gram (RE) of carbon dioxide liquefied, which is 3.39× more efficient compared with an RE of 8.48 W-hr/g reported by Muscatello et al. (Muscatello et al. (2015).

The collected carbon dioxide expands through an adiabatic valve and heat exchanger to 0.13523 MPa and 583.15 K and is fed into the Sabatier subsystem at 0.52 g/s initially. Preliminary calculations show that the heated valve delivers 390.85 W of heat to the passing gas while raising its temperature by 310 K. Hydrogen passes via a mixing box to a heat exchanger where it heats up to the Sabatier reactor temperature of 583.15 K. The heat exchanger energy balance reveals that 551.76 W of heat is gained by hydrogen to raise its temperature. The mass flow rates of both hydrogen and carbon dioxide are limited by the hydrogen-carbon molar ratio (of 4) required to sustain the Sabatier reaction. Inside the Sabatier reactor, hydrogen and carbon dioxide react to form a gaseous mixture of methane, carbon monoxide, carbon dioxide, hydrogen, and water. The exothermicity of the ensuing reaction generates approximately 1.97 kW of heat.

Due to the difficulty associated with the extraction of water and carbon dioxide on Mars, the exhaust gases from the Sabatier block are recycled to maximize methane production. However, it can be difficult to measure H_2 concentration in the gaseous mixture entering the Sabatier catalyst, and inaccurate measurements of H_2 can influence the CO_2/H_2 ratio and lower catalyst efficiency. Therefore, the separation of these gases is assumed necessary while potentially supporting other aspects of a colony. After separation, pure carbon dioxide can be used to produce high purity oxygen as demonstrated by Sanders et al. (Sanders et al. (2014). Bleeding off pure carbon dioxide for oxygen production can potentially help maintain the CO_2/H_2 ratio necessary to maintain optimum methane production in the Sabatier catalyst. Pure hydrogen can also be utilized either in fuel cells for auxiliary power generation or as a feedstock for liquid hydrogen or hydrazine rocket fuel. Pure CO_2 and H_2 streams can be monitored relatively accurately and could provide unhindered operation at higher efficiencies.

There are two fluid separation stages—the first stage involves the removal of water from the stream, whereas the second stage employs PSA to capture CH_4, CO_2, and H_2 from the mixture. In the first stage, water is recovered from the stream via cooling and condensation, as it can deactivate the PSA catalyst and reduce its efficiency. The cooling stage rejects around 1.57 kW of heat into the ambient that cools

the gases to 273.15 K (temperature of water storage tank). This promotes water vapor condensation and subsequent collection in the water tank. After the removal of water, the *dry* gases undergo compression to reach the PSA system conditions (1.83 MPa [Sircar and Golden, 2000]) that require 420.50 W of compression work. As the gas mixture temperature rises to 597.11 K during compression, a heat exchanger is employed to lower it down to 294.15 K (PSA temperature), resulting in the rejection of 398.25 W of heat to the ambient. The exiting gases are fed into a PSA unit where hydrogen and carbon dioxide are recovered as much as possible, and the remaining gases are sent to the methane liquefaction unit. Because hydrogen needs to be recycled through the heat exchanger employed between the electrolysis and Sabatier blocks, it is passed through a valve to lower its pressure to match the heat exchanger's pressure. Carbon dioxide is compressed at the expense of 129.51 W to raise its pressure to that of the adiabatic heated valve employed before the Sabatier block. The gaseous mixture M3, which primarily consists of methane, is compressed to 3.49 MPa, costing the system 246.25 W. Subsequently, a heat exchanger rejects 267.01 W of heat to cool down the gases to 273.15 K, yielding liquid carbon dioxide.

After carbon dioxide separation and collection in the tank along with atmospherically collected carbon dioxide, the reverse analysis of the system finds that 9.14 MPa pressure in the heat exchanger balances the valve energy equation. Then, methane liquefies and is stored at 112.6 K and 0.109 MPa, whereas the remaining trace amounts of hydrogen and carbon monoxide are purged into the ambient. The compressor used to raise the incoming gases to 9.14 MPa consumes 42.89 W of electricity.

DISCUSSION

Along with the temperature, pressure, and mass flow rate data at each State, it is important to provide the heat, work, and entropy values. Although heat and work results are critical from the standpoint of system performance, the entropy values help evaluate the system and its components through the lens of thermodynamics' second law to provide a feasibility check. The subsystem heat, work, and entropy generation results are presented in Table 3. A quick heat balance of all systems reveals that the overall system loses approximately 95.03 kW of useful heat into the ambient. As mentioned prior, the system can be optimized to reuse this heat for other processes. Positive entropy generation in all processes shows that their thermodynamic analysis is theoretically consistent, and scaling them to real-world experiments could be possible in the future. Because some components of the system, such as heated valves, require a continuous heat supply, their entropy generation was calculated assuming that the heat source is held at 1000 K. It is worth mentioning here that the use of accurate source temperatures (where known) would make this analysis more correct.

Table 3 shows that the compressor work during oxygen liquefaction (State 9–10 of Figure 3) is significantly large from the standpoint of operation on Mars. A sensitivity analysis was conducted to determine the influence of the liquid oxygen storage temperature on compressor work. Table 4 shows that increasing the storage temperature of liquid oxygen grows the vapor quality of the fluid. In other words, the liquid fraction of oxygen in the loop diminishes while the gaseous fraction grows. More work is then required to compress the increased gaseous mass (in the loop) to the desired pressure. Minimizing the LO_x storage temperature should be a priority to reduce power requirements.

Overall, it may become increasingly difficult to generate electricity to meet this power requirement. A total energy requirement of approximately 34.3 kW is estimated by summing up the energy requirements of the electrolysis (Table 3) and liquid oxygen storage (Table 4 @ 200 K) processes. Because research shows that the continuous power demand on Mars ranges from 4 to 100 kW with an average of 40 kW (Abel et al., 2021; Anderson et al., 2018), effectively doubling this power would be necessary to keep the system in operation. To help minimize energy requirements, future work can build on this effort by investigating the influence of diurnal and seasonal temperature swings on liquid methane and oxygen production in combination with advanced heat transfer and energy storage options, such as heat pipes (Zhang et al., 2020) and phase change materials (Kansara and Singh, 2021).

As a proof of concept, Table 5 shows that the 16-month (1.332 years) target set forth by NASA to refuel rockets on Mars can be readily met with the currently achievable flow rates of liquid methane and liquid oxygen. In contrast, completely refueling a Starship (SpaceX) on Mars would take longer than 50 years and does not appear attractive. The use of 38 such ISRU systems operating in parallel could potentially refuel a Starship within 16 months (16 months for methane refueling, 10 months for oxygen refueling); this implies that the current ISRU system is capable of meeting the refueling time targets, and scaling it could further reduce the refueling times significantly.

Table 3. Heat, work, and entropy generation from major subsystems

Block	Process	Mechanical component	$\dot{Q}$ (W)	$\dot{W}$(W)	$\dot{\sigma}$(W/K)
Water mining	1	Reactor	—	−340.00	—
Atmospheric CO_2 collection	3–2	Reactor	—	−50.00	—
Electrolysis	5-6-7	Reactor	—	−21,130.04	9.92
O_2 liquefaction	6-14-9	MB	—	—	0.03
	9–10	Compressor	—	−69,778.06	18.43
	10–11	HX	−76,692.45	—	231.38
	11–12	EV	—	—	66.49
	13–14	HX	6,546.64	—	14.52
Sabatier + H_2 and CO_2 Recycle	7-26-17	HX	679.31	—	0.97
	16-17-18	Reactor	−1,973.80	—	4.62
	18-19-20	Condenser	−1,567.20	—	3.73
	20–21	Compressor	—	−420.50	0.23
	21–22	HX	−398.26	—	0.98
	22-23-24–25	Separator	—	−1.84	0.25
	23–26	EV	—	—	0.33
	24–27	Compressor	—	−129.51	0.06
	15-27-16	HV	262.91	—	1.08
CH_4 liquefaction	25–28	Compressor	—	−246.25	0.11
	28-29-30	HX	−267.01	—	0.69
	29–31	Compressor	—	−42.89	0.04
	31–32	HX	−104.86	—	0.11
	32–33	EV	—	—	0.34

MB: Mixing box.
HX: Heat exchanger.
EV: Expansion valve.
HV: Heated valve

Table 5 indicates that a significant mass of Martian regolith needs to be moved per day to meet SpaceX deadlines for propellant production. Establishing the ISRU system near Mars' poles could potentially leverage a greater water ice content and help maximize the water flow rates, thus boosting system efficiency. It is reported that CO_2 solidifies at higher latitude regions during Martian winters due to low temperatures (Leighton and Murray, 1966), and the thickness of this CO_2 ice cover increases with proximity to the poles (Aharonson, 2004). Because CO_2 ice is heavier than H_2O ice, it may potentially cause equipment failure, and one of the Phoenix's solar panels might have snapped from this CO_2 ice accumulation (Wall, 1981). The CO_2 ice cover could also hinder auger operation during the winter months (Zacny et al., 2012). Therefore, exploring the more benign equatorial regions for ISRU and human post establishment appears desirable.

Conclusions

The presence of carbon, hydrogen, and oxygen compounds on Mars makes an interesting argument to investigate the possibility of *in-situ* production of rocket propellants for return or extended deep-space

Table 4. Effect of liquid oxygen storage temperature on vapor quality and compressor work

LO_x storage temperature (K)	Vapor quality (−)	$\dot{W}_{9-10}$ (W)	% change (from 200 K case)
200	0.9097	−11,894.90	—
203.15	0.9333	−16,139.03	35.68
210	0.9841	−69,778.06	486.62

Table 5. Propellant refueling targets set forth by NASA and SpaceX for rockets on Mars

Refueling	Company	Target mass [tonnes]	Deadline	Refueling time [year]	Status
Methane	NASA	7	16 months (or 1.332 years	1.32	Meets expectations
	SpaceX	267	N.A.	50.35	NA
Oxygen	NASA	22	16 months (or 1.332 years	0.71	Meets expectations
	SpaceX	933	N.A.	30.27	N.A.

For sustained operation, the required regolith movement for NASA and SpaceX is 65 kg/day and 2496 kg/day, respectively.

missions. Although *in-situ* production of methane on Mars has been proposed earlier, there is a lack of system feasibility studies in the available literature due to perfect approximations for devices such as a Sabatier reactor. To fill this void, a system capable of extracting carbon dioxide from the Martian atmosphere and water from its regolith for *in-situ* methane production on Mars was modeled in Matlab and explored from the standpoint of thermodynamics. The model simulates system performance for the achievable ice and carbon dioxide extraction rates on Mars and evaluates their impact on the liquid oxygen and liquid methane production rates. Based on the second law of thermodynamics, the assessment of the current system emerges as a TRL 3 proof of concept and reveals that an *in-situ* system for propellant production on Mars is potentially possible. The model shows that at the current achievable flow rates of CO_2 and water, it is possible to meet NASA's 16-month deadline for refueling rockets on Mars. Due to the dynamic nature of the model, it can be scaled further to meet tighter rocket refueling deadlines. A major facet of the current effort is the use of Martian nighttime temperatures for heat exchange that can potentially reduce the dependence on power-hungry cryogenic methods for gas liquefaction.

Limitations of the study

Although the current system is based on existing technology, it can use real-world efficiencies for a more accurate analysis. It becomes imperative to include specifics from actual processes, such as industrial use of electrolysis, to generate hydrogen. It would be useful to update the system inlet mass flow rates with data from recent Martian water and CO_2 capture efforts as more progress is made. As the overall system is sensitive to minor perturbations in liquid oxygen storage temperature where a small change in the oxygen storage temperature from 200 K to 210 K can increase compressor work by 4.86×, state temperatures and pressures must be carefully selected to minimize power requirements. The model can also be used to assess the influence of Martian diurnal and seasonal temperature variations on the system performance. This includes a comparison of using pure CO_2 and H_2 streams for the Sabatier process versus using the Martian atmosphere directly to minimize energy usage. Such efforts will be beneficial for other research efforts that are focused on energy infrastructure and supply chains for Mars. Overall, expanding the scope of the current model can assist the corresponding experimental investigation to potentially achieve higher TRL ratings.

STAR★METHODS

Detailed methods are provided in the online version of this paper and include the following:

- KEY RESOURCE TABLE
- RESOURCE AVAILABILITY
  - Lead contact
  - Materials availability
  - Data and code availability
- METHOD DETAILS
  - Chemical species normalization
  - Governing equations

ACKNOWLEDGMENTS

This work was supported by the National Aeronautics and Space Administration via grant number 80NSSC19M0042.

AUTHOR CONTRIBUTIONS

Conceptualization, C. D.; Methodology, C.D. and S.S.A.; Software, C.D. and S.S.A.; Validation, C.D. and S.S.A.; Formal Analysis, C.D. and S.S.A.; Investigation, C.D. and S.S.A.; Resources, C.D., S.P.B., and J.H.; Data Curation, S.S.A. and C.D.; Writing—Original Draft, S.S.A.; Writing—Review and Editing, S.S.A., C.D., S.P.B., J.H., and E.M.D.; Visualization, S.S.A.; Supervision, C.D.; Project Administration, S.P.B., C.D., and J.H.; Funding Acquisition, S.P.B., C.D., and J.H.

DECLARATION OF INTERESTS

All authors declare that there are no competing interests.

Received: January 19, 2022
Revised: April 6, 2022
Accepted: April 22, 2022
Published: May 20, 2022

REFERENCES

Abel, A.J., Berliner, A.J., Mirkovic, M., Collins, W.D., Arkin, A.P., and Clark, D.S. (2021). Photovoltaics-driven power production can support human exploration on Mars. Preprint at arXiv. https://doi.org/10.48550/arXiv.2110.14757.

Adan-Plaza, S., Carpenter, K., Elias, L., Grover, R., Hilstad, M., Hoffman, C., Schneider, M., and Bruckner, A. (1998). Extraction of Atmospheric Water on Mars for the Mars Reference Mission, p. 171. https://www.lpi.usra.edu/publications/reports/CB-955/washington.pdf.

Aharonson, O. (2004). Depth, distribution, and density of CO_2 deposition on Mars. J. Geophys. Res. *109*, E05004. https://doi.org/10.1029/2003je002223.

Alam, S.S., and Depcik, C. (2019). Verification and validation of a homogeneous reaction kinetics model using a detailed H2-O2 reaction mechanism versus chemkin and cantera. Eng. Education *5*. https://doi.org/10.1115/imece2019-10028.

Anderson, M.S., Ewert, M.K., and Keener, J.F. (2018). Life support baseline Values and assumptions document. NASA report. https://ntrs.nasa.gov/api/citations/20180001338/downloads/20180001338.pdf.

Ash, R.L., Dowler, W.L., and Varsi, G. (1978). Feasibility of rocket propellant production on Mars. Acta Astronautica *5*, 705–724. https://doi.org/10.1016/0094-5765(78)90049-8.

Chen, H., Sarton du Jonchay, T., Hou, L., and Ho, K. (2020). Integrated in-situ resource utilization system design and logistics for Mars exploration. Acta Astronautica *170*, 80–92. https://doi.org/10.1016/j.actaastro.2020.01.031.

Clapp, M. (1991). Comparison of mars-produced Methane and carbon monoxide (27th Joint Propulsion Conference). https://doi.org/10.2514/6.1991-2442.

Depcik, C. (2018). Exploring the Potential of Combustion on Titan. SAE Int. J. Aerosp. *11*. 01-11-01-0002-46. https://doi.org/10.4271/01-11-01-0002.

England, C. (2001). Mars Atmosphere Resource Recovery System (MARRS) (39th Aerospace Sciences Meeting and Exhibit). https://doi.org/10.2514/6.2001-942.

Falbo, L., Visconti, C.G., Lietti, L., and Szanyi, J. (2019). The Effect of CO on CO_2 methanation over Ru/Al_2O_3 catalysts: a combined steady-state Reactivity and transient DRIFT spectroscopy study. Appl. Catal. B Environ. *256*, 117791. https://doi.org/10.1016/j.apcatb.2019.117791.

Franz, H.B., Trainer, M.G., Malespin, C.A., Mahaffy, P.R., Atreya, S.K., Becker, R.H., Benna, M., Conrad, P.G., Eigenbrode, J.L., Freissinet, C., et al. (2017). Initial SAM calibration gas experiments on Mars: quadrupole mass spectrometer results and implications. Planet. Space Sci. *138*, 44–54. https://doi.org/10.1016/j.pss.2017.01.014.

Frontera, P., Macario, A., Ferraro, M., and Antonucci, P. (2017). Supported Catalysts for CO_2 methanation: a Review. Catalysts *7*, 59. https://doi.org/10.3390/catal7020059.

Garbarino, G., Bellotti, D., Riani, P., Magistri, L., and Busca, G. (2015). Methanation of carbon Dioxide on Ru/Al_2O_3 and Ni/Al_2O_3 Catalysts at atmospheric pressure: catalysts activation, Behaviour and stability. Int. J. Hydrogen Energy *40*, 9171–9182. https://doi.org/10.1016/j.ijhydene.2015.05.059.

Grima, C., Kofman, W., Mouginot, J., Phillips, R.J., Hérique, A., Biccari, D., Seu, R., and Cutigni, M. (2009). North polar deposits of Mars: extreme purity of the water ice. Geophys. Res. Lett. *36*. https://doi.org/10.1029/2008gl036326.

Guerra, L., Rossi, S., Rodrigues, J., Gomes, J., Puna, J., and Santos, M.T. (2018). Methane production by a combined sabatier reaction/water electrolysis process. J. Environ. Chem. Eng. *6*, 671–676. https://doi.org/10.1016/j.jece.2017.12.066.

Heldmann, J.L., Marinova, M.M., Lim, D.S.S., Wilson, D., Carrato, P., Kennedy, K., Esbeck, A., Anthony Colaprete, T., Elphic, R.C., Captain, J., et al. (2021). Mission architecture using the SpaceX starship vehicle to enable a sustained human presence on Mars. New Space. https://doi.org/10.1089/space.2020.0058.

Johnson, W.L., Hauser, D.M., Plachta, D.W., Wang, X.Y.J., Banker, B.F., Desai, P.S., Stephens, J.R., and Swanger, A.M. (2018). Comparison of oxygen liquefaction methods for use on the martian surface. Cryogenics *90*, 60–69. https://doi.org/10.1016/j.cryogenics.2017.12.008.

Kansara, K., and Singh, V.K. (2021). Effect of heat source direction on the thermal performance of phase change material (PCM) based thermal control module (TCM) under the influence of low gravity environment. Int. Commun. Heat Mass Transfer *128*, 105615. https://doi.org/10.1016/j.icheatmasstransfer.2021.105615.

Landis, G.A., and Linne, D.L. (2001). Mars rocket vehicle using in situ propellants. J. Spacecraft Rockets *38*, 730–735. https://doi.org/10.2514/2.3739.

Leighton, R.B., and Murray, B.C. (1966). Behavior of carbon dioxide and other volatiles on Mars. Science *153*, 136–144. https://doi.org/10.1126/science.153.3732.136.

Leucht, K.W. (2018). How NASA will use robots to create rocket fuel on Mars: the year is 2038. IEEE Spectr. *55*, 34–39. https://doi.org/10.1109/mspec.2018.8513782.

Linne, D., Groth, M., and Roncace, J. (1990). Mars in situ propellants - carbon Monoxide and oxygen ignition experiments (26th Joint Propulsion Conference). https://doi.org/10.2514/6.1990-1894.

Linne, D.L., and Kleinhenz, J.E. (2016). Extraction and Capture of Water from Martian Regolith Experimental Proof-Of-Concept (8th Symposium on Space Resource Utilization). https://doi.org/10.2514/6.2016-0226.

Liu, J., Li, H., Sun, L., Guo, Z., Harvey, J., Tang, Q., and Jia, M. (2021). In-situ resources for infrastructure construction on Mars: a Review. Int. J. Transport. Sci. Technol. *11*, 1–16. https://doi.org/10.1016/j.ijtst.2021.02.001.

Malara, A., Frontera, P., Antonucci, P., and Macario, A. (2020). Smart recycling of carbon oxides: current status of methanation reaction. Curr. Opin. Green Sustain. Chem. *26*, 100376. https://doi.org/10.1016/j.cogsc.2020.100376.

Moioli, E., and Züttel, A. (2020). A model-based comparison of Ru and Ni catalysts for the sabatier

reaction. Sustain. Energy Fuels *4*, 1396–1408. https://doi.org/10.1039/c9se00787c.

Muscatello, A., Devor, R., and Captain, J. (2015). Atmospheric processing module for Mars propellant production. Earth and Space. https://doi.org/10.1061/9780784479179.047.

Muscatello, A.C., Santiago-Maldonado, E., Gibson, T., Devor, R., and Captain, J. (2011). Evaluation of Mars CO_2 Capture and gas separation technologies. NASA report. https://ntrs.nasa.gov/api/citations/20110015862/downloads/20110015862.pdf.

National Aeronautics and Space Administration (2012). Technology Readiness Level. https://www.nasa.gov/directorates/heo/scan/engineering/technology/technology_readiness_level.

National Institute of Standards and Technology (2013). REFPROP | NIST. https://www.nist.gov/srd/refprop.

Palmer, C. (2021). SpaceX starship lands on Earth, but manned missions to Mars will require more. Engineering *7*, 1345–1347. https://doi.org/10.1016/j.eng.2021.08.005.

Park, J., Kang, R.H., and Lee, J.W. (2017). Efficient pressure swing Adsorption for improving H_2 Recovery in precombustion CO_2 capture. Korean J. Chem. Eng. *34*, 1763–1773. https://doi.org/10.1007/s11814-017-0080-7.

Pickett, M.T., Roberson, L.B., Calabria, J.L., Bullard, T.J., Turner, G., and Yeh, D.H. (2020). Regenerative water purification for space applications: needs, challenges, and technologies towards 'closing the loop. Life Sci. Space Res. *24*, 64–82. https://doi.org/10.1016/j.lssr.2019.10.002.

Prydz, R., and Goodwin, R.D. (1972). Experimental melting and vapor pressures of methane. J. Chem. Thermodyn. *4*, 127–133. https://doi.org/10.1016/s0021-9614(72)80016-8.

Reddig, M., and MacKnight, A. (1997). Investigation of Mars In-Situ Propellant Production (SAE Technical Paper Series). https://doi.org/10.4271/972496.

Rönsch, S., Schneider, J., Matthischke, S., Schlüter, M., Götz, M., Lefebvre, J., Prabhakaran, P., and Bajohr, S. (2016). Review on methanation - from fundamentals to current projects. Fuel *166*, 276–296. https://doi.org/10.1016/j.fuel.2015.10.111.

Salerno, L.J., and Kittel, P. (1999). Cryogenics and the human exploration of Mars. Cryogenics *39*, 381–388. https://doi.org/10.1016/s0011-2275(99)00043-0.

Sanders, G.B., Araghi, K., Ess, K., Valencia, L., Muscatello, A.C., Calle, C., Clark, D.L., and Iacomini, C.S. (2014). Mars atmosphere resource verification INsitu (MARVIN) - in situ resource demonstration for the Mars 2020 mission (AIAA SPACE 2014 Conference and Exposition). https://doi.org/10.2514/6.2014-4235.

Sanders, G.B., Paz, A., Oryshchyn, L., Araghi, K., Muscatello, A., Linne, D.L., Kleinhenz, J.E., and Peters, T. (2015). Mars ISRU for production of mission critical consumables - options, recent studies, and current state of the art (AIAA SPACE 2015 Conference and Exposition). https://doi.org/10.2514/6.2014-4458.

Sheehan, S.W. (2021). Electrochemical methane Production from CO_2 for Orbital and interplanetary refueling. iScience *24*, 102230. https://doi.org/10.1016/j.isci.2021.102230.

Shishko, R., Fradet, R., Do, S., Saydam, S., Tapia-Cortez, C., Dempster, A.G., and Coulton, J. (2017). Mars colony in situ resource utilization: an integrated architecture and economics model. Acta Astronautica *138*, 53–67. https://doi.org/10.1016/j.actaastro.2017.05.024.

Sircar, S. (2002). Pressure swing adsorption. Ind. Eng. Chem. Res. *41*, 1389–1392. https://doi.org/10.1021/ie0109758.

Sircar, S., and Golden, T.C. (2000). Purification of hydrogen by pressure swing adsorption. Sep. Sci. Technol. *35*, 667–687. https://doi.org/10.1081/ss-100100183.

Spanovich, N., Smith, M.D., Smith, P.H., Wolff, M.J., Christensen, P.R., and Squyres, S.W. (2006). Surface and near-surface atmospheric temperatures for the Mars exploration rover landing sites. Icarus *180*, 314–320. https://doi.org/10.1016/j.icarus.2005.09.014.

Stangeland, K., Kalai, D., Li, H., and Yu, Z. (2017). CO_2 methanation: the Effect of Catalysts and reaction conditions. Energy Proced. *105*, 2022–2027. https://doi.org/10.1016/j.egypro.2017.03.577.

Starr, S.O., and Muscatello, A.C. (2020). Mars in situ resource utilization: a Review. Planet. Space Sci. *182*, 104824. https://doi.org/10.1016/j.pss.2019.104824.

Su, X., Xu, J., Liang, B., Duan, H., Hou, B., and Huang, Y. (2016). Catalytic carbon dioxide hydrogenation to methane: a Review of recent studies. J. Energy Chem. *25*, 553–565. https://doi.org/10.1016/j.jechem.2016.03.009.

Sullivan, T.A., Linne, D., Bryant, L., and Kennedy, K. (1995). In-situ-produced methane and methane/carbon monoxide mixtures for return propulsion from Mars. J. Propulsion Power *11*, 1056–1062. https://doi.org/10.2514/3.23935.

Todd, D., Schwager, M., and Mérida, W. (2014). Thermodynamics of high-temperature, high-pressure water electrolysis. J. Power Sources *269*, 424–429. https://doi.org/10.1016/j.jpowsour.2014.06.144.

Ursua, A., Gandia, L.M., and Sanchis, P. (2012). Hydrogen production from water electrolysis: current status and future trends. Proc. IEEE *100*, 410–426. https://doi.org/10.1109/jproc.2011.2156750.

Voldsund, M., Jordal, K., and Anantharaman, R. (2016). *Hydrogen Production with CO_2 capture*. Int. J. Hydrogen Energy *41*, 4969–4992. https://doi.org/10.1016/j.ijhydene.2016.01.009.

Wall, S.D. (1981). Analysis of condensates formed at the viking 2 lander site: the first winter. Icarus *47*, 173–183. https://doi.org/10.1016/0019-1035(81)90165-2.

Wang, W., Wang, S., Ma, X., and Gong, J. (2011). Recent advances in catalytic hydrogenation of carbon dioxide. Chem. Soc. Rev. *40*, 3703. https://doi.org/10.1039/c1cs15008a.

Wiens, J., Bommarito, F., Blumenstein, E., Ellsworth, M., Cisar, T., McKinney, B., and Knecht, B. (2001). Water Extraction from Martian Soil (Fourth Annual HEDS-UP Forum), pp. 11–25. https://www.lpi.usra.edu/publications/reports/CB-1106/csm01.pdf.

Wiessner, F.G. (1988). Basics and industrial applications of pressure swing adsorption (PSA), the modern way to separate gas. Gas Sep. Purif. *2*, 115–119. https://doi.org/10.1016/0950-4214(88)80026-4.

Wiheeb, A.D., Helwani, Z., Kim, J., and Othman, M.R. (2015). Pressure swing adsorption technologies for carbon dioxide capture. Sep. Purif. Rev. *45*, 108–121. https://doi.org/10.1080/15422119.2015.1047958.

Yan, Z., Hitt, J.L., Turner, J.A., and Mallouk, T.E. (2019). Renewable electricity storage using electrolysis. Proc. Natl. Acad. Sci. U S A *117*, 12558–12563. https://doi.org/10.1073/pnas.1821686116.

Zacny, K., Chu, P., Paulsen, G., Avanesyan, A., Craft, J., and Osborne, L. (2012). Mobile in-situ water extractor (MISWE) for Mars, moon, and asteroids in situ resource utilization. In AIAA SPACE 2012 Conference & Exposition. https://doi.org/10.2514/6.2012-5168.

Zhang, W., Zhang, D., Wang, C., Tian, W., Qiu, S., and Su, G.H. (2020). Conceptual design and analysis of a megawatt power level heat pipe cooled space reactor power system. Ann. Nucl. Energy *144*, 107576. https://doi.org/10.1016/j.anucene.2020.107576.

Zhu, X., Li, S., Shi, Y., and Cai, N. (2019). Recent advances in elevated-temperature pressure swing adsorption for carbon capture and hydrogen production. Prog. Energy Combust. Sci. *75*, 100784. https://doi.org/10.1016/j.pecs.2019.100784.

Zubrin, R., Muscatello, T., Birnbaum, B., Caviezel, K., Snyder, G., and Berggren, M. (2002). Progress in Mars ISRU Technology (40th AIAA Aerospace Sciences Meeting & Exhibit). https://doi.org/10.2514/6.2002-461.

STAR★METHODS

KEY RESOURCE TABLE

REAGENT or RESOURCE	SOURCE	IDENTIFIER
Deposited data		
Simulation results	This paper	Table 5
Software and algorithms		
Matlab-based ISRU thermodynamic model	This paper.	Available at Github, https://github.com/depcik/mars/

RESOURCE AVAILABILITY

Lead contact

Further information and requests for data should be directed to and will be fulfilled by the lead contact, Dr. Christopher Depcik (depcik@ku.edu).

Materials availability

This study did not generate new unique reagents.

Data and code availability

- All relevant data have been deposited at Github and are publicly available at https://github.com/depcik/mars as of the date of publication.
- All original code has been deposited at https://github.com/depcik/mars and is publicly available as of the date of publication.
- Any additional information required to reanalyze the data reported in this paper is available from the lead contact upon request.

METHOD DETAILS

The thermodynamic analysis of the proposed system depends on the formulation of a system of equations comprised of fundamental conservation equations. Before analyzing the system, it is important to normalize all species to a common datum to eliminate any errors arising due to the different methodologies involved in determining their state properties.

Chemical species normalization

The thermodynamic and transport properties of all working fluids in the system are handled by the Reference Fluid Thermodynamic and Transport Properties Database (REFPROP10), a one-stop solution prepared by the National Institute of Standards and Technology (NIST) (NIST 2013). The reference states of the species included in this database might vary due to the different experimental methodologies behind the determination of these properties. Fluid properties, such as enthalpy and entropy, of all species were normalized to the standard NIST conditions of 298.15 K and 1 atm to provide a common datum for the thermodynamic calculations. A similar effort by Depcik to explore the potential of combustion on Titan, the moon of Saturn, was used as the template for the normalization efforts (Depcik, 2018).

Governing equations

This section provides an insight into the common assumptions used to simplify the governing equations that were used to model and evaluate system performance. The conservation of mass governs the flow in ($\dot{m}_{inlet}$) and out ($\dot{m}_{exit}$) of each component of the system in Figure 3.

$$\frac{dm_{CV}}{dt} + \sum_{exit} \dot{m}_{exit} - \sum_{inlet} \dot{m}_{inlet} = 0 \quad \left[\frac{kg}{s}\right] \qquad \text{(Equation 5)}$$

where $\frac{dm_{CV}}{dt}$ is the rate of change of the mass inside the control volume. Typical assumptions present are that the systems are modeled as steady-state with their behavior remaining constant with respect to time and that the flows in and out of each device are one-dimensional.

Generally, the conservation of momentum equation is not indicated explicitly when describing thermodynamic systems:

$$F = \frac{d}{dt}(m \cdot V) \quad [N] \qquad \text{(Equation 6)}$$

It is embedded within the analysis by assuming constant pressure devices as a balance of flow forces (F) with no viscous losses in a steady-state situation removing the change in momentum ($m \cdot V$) with respect to time. This effort makes the same assumption, but it is pertinent to indicate this equation's importance as others might wish to include pressure drops through the devices.

The steady-state and one-dimensional flow assumptions for the thermodynamic systems simplify both the energy and entropy equations. The energy equation was simplified further by neglecting the kinetic and potential energy terms. Specific assumptions for some systems, including adiabatic conditions for compressors and valves along with no power for heat exchangers and mixing boxes also contributed to the simplification.

$$0 = \dot{Q}_{CV} - \dot{W}_{CV} + \sum_{in} \dot{m}_i h_i - \sum_{ex} \dot{m}_j h_j \quad [W] \qquad \text{(Equation 7)}$$

where $_{Qcv}$ signifies the rate of heat transfer through the system (0 for adiabatic assumption), $\dot{W}_{cv}$ is the work term (includes expansion and compression work), $\dot{m}$ is the mass flow rate of a flow, and h is the enthalpy of the flow. The subscripts i and j denote the number of flows entering (*in*) or leaving (*ex*) the system, respectively.

The previously mentioned assumptions yield the following form of the second law of thermodynamics:

$$0 = \frac{\dot{Q}_{CV}}{T} + \sum_{in} \dot{m}_i s_i - \sum_{ex} \dot{m}_j s_j + \dot{\sigma}_{CV} \quad \left[\frac{W}{K}\right] \qquad \text{(Equation 8)}$$

where T is the surrounding temperature, s is the mass-specific entropy of the fluids entering or leaving the system and σ_{CV} is the entropy generation in the system. The subscripts i, j, *in*, and *ex* retain their meanings from the energy equation. The entropy equation was employed for compressors to utilize an assumed compressor isentropic efficiency. The entropy equation also serves as a *check* to ensure that the calculations provide a *thermodynamically* possible result. All equations were solved in Matlab with REFPROP10 providing the state properties.